Cancer Cell
Article

A Mouse Model of the Most Aggressive Subgroup of Human Medulloblastoma

Daisuke Kawauchi,[1,7] Giles Robinson,[2,7] Tamar Uziel,[1,8] Paul Gibson,[5] Jerold Rehg,[3] Cuilan Gao,[4] David Finkelstein,[4] Chunxu Qu,[6] Stanley Pounds,[4] David W. Ellison,[3] Richard J. Gilbertson,[5,*] and Martine F. Roussel[1,*]
[1]Department of Tumor Cell Biology
[2]Department of Oncology
[3]Department of Pathology
[4]Department of Biostatistics
[5]Department of Developmental Neurobiology
[6]Department of Information Sciences
St. Jude Children's Research Hospital, 262 Danny Thomas Place, Memphis, TN 38105, USA
[7]These authors contributed equally to this work
[8]Present address: Global Pharmaceutical Research and Development—Cancer Research, Abbott Laboratories, 100 Abbott Park Road, Building AP-10, Room 201, Abbott Park, IL 60064, USA
*Correspondence: martine.roussel@stjude.org (M.F.R.), richard.gilbertson@stjude.org (R.J.G.)
DOI 10.1016/j.ccr.2011.12.023

SUMMARY

Medulloblastomas that display a large cell/anaplastic morphology and overexpress the cellular *c-MYC* gene are highly aggressive and carry a very poor prognosis. This so-called MYC-subgroup differs in its histopathology, gene expression profile, and clinical behavior from other forms of medulloblastoma. We generated a mouse model of MYC-subgroup medulloblastoma by transducing *Trp53*-null cerebellar progenitor cells with *Myc*. The cardinal features of these mouse medulloblastomas closely mimic those of human MYC-subgroup tumors and significantly differ from mouse models of the Sonic-Hedgehog- and WNT-disease subgroups. This mouse model should significantly accelerate understanding and treatment of the most aggressive form of medulloblastoma and infers distinct roles for *MYC and MYCN* in tumorigenesis.

INTRODUCTION

Medulloblastoma (MB)—the most common malignant pediatric brain tumor—includes at least four clinically and molecularly distinct subgroups (Cho et al., 2011; Kool et al., 2008; Northcott et al., 2011; Thompson et al., 2006). Sonic Hedgehog (SHH)-subgroup MB most frequently results from inactivating mutations of PTCH1 (the SHH receptor) or suppressor of fused (a downstream signal transducer). SHH signaling ultimately activates GLI family transcription factors that upregulate pro-proliferative genes, such as *MYCN*, *CCND1*, and *CCND2* (cyclins D1 and D2), and lead to the reduced expression of inhibitors of cyclin-dependent kinases (CDKs), including $p27^{KIP1}$ and $p18^{INK4c}$ (Roussel and Hatten, 2011). About 50% of SHH-subgroup MBs exhibit a desmoplastic/nodular histology and carry an intermediate prognosis in patients who receive contemporary surgical intervention and chemotherapy (Cho et al., 2011; Ellison et al., 2011a; Lam et al., 1999; Northcott et al., 2011; Raffel et al., 1997). In contrast, the WNT-subgroup disease has an excellent prognosis, exhibits a "classic" morphology, and is frequently triggered by mutations in the WNT pathway effector CTNNB1 (β-catenin; Cho et al., 2011; Ellison et al., 2005; Gajjar et al., 2006; Kool et al., 2008; Northcott et al., 2011; Thompson et al., 2006). An interesting distinction between SHH- and WNT-driven MBs is their anatomic location, with SHH tumors arising laterally in the cerebellum and WNT MBs arising in the midline close to the brainstem; recent results indicate that these features reflect

Significance

MYC-subgroup medulloblastoma (MB) is one of the most aggressive pediatric brain tumors. This disease is resistant to combination surgery, radiotherapy, and chemotherapy and kills most affected children within three years of diagnosis. Mouse models of the Sonic Hedgehog and WNT forms of MB have advanced understanding of the biology and treatment of these disease subgroups. In contrast, the absence of preclinical models of MYC-driven MB has limited understanding of this important tumor. Here, we describe the MYC-driven mouse model of MB that accurately mimics the transcriptome, histopathology, and clinical behavior of human MYC-subgroup disease. This model should significantly advance efforts to develop therapeutic modalities and determine the origin of this deadly childhood cancer.

the different cells of origin of the two MB subgroups (Gibson et al., 2010).

Modeling both the SHH- and WNT-subgroups of MB in the mouse (Wu et al., 2011) has been instrumental in providing insights into the cellular origins of these different disease forms and paving the way for therapeutic development (Romer et al., 2004). SHH-subgroup MBs arise within the cerebellum from committed, SHH-dependent granule neuron precursors (GNPs; Schüller et al., 2008; Yang et al., 2008). Very recently, we demonstrated that WNT-subgroup MBs arise outside of the cerebellum from progenitor cells in the lower rhombic lip (Gibson et al., 2010). Thus, subgroups of MB are likely to reflect intrinsically different diseases with distinct origins and driver mutations.

In contrast to the SHH- and WNT-subgroups, very little is known about the molecular aberrations that drive two other subgroups of the disease. Non-SHH/WNT tumors include the most aggressive form of the disease (MYC-subgroup) that exhibits frequent amplification and/or overexpression of *MYC,* portends a dismal prognosis, and generates a high proportion of aggressive and invasive tumors with large cell/anaplastic (LC/A) histology (Cho et al., 2011; Ellison et al., 2011a; Northcott et al., 2011; Pfister et al., 2009).

Mycn is a critical mediator of SHH signals in GNPs (Kenney et al., 2003) and is absolutely required for normal cerebellar development; however, much less is known about the function of Myc in the mouse hindbrain (Knoepfler et al., 2002; Zindy et al., 2006). Myc is not normally expressed in GNPs (Zindy et al., 2006), and overexpression of *MYC* and *MYCN* is mutually exclusive and associated with distinct subgroups of human MBs (Cho et al., 2011; Northcott et al., 2011). High-level expression and amplification of *MYCN* are observed across the various subgroups of human MB. Aberrant activation of *Mycn* expression in the developing mouse cerebellum initiates a variety of MBs, including both classic and LC/A tumors (Swartling et al., 2010). In contrast, the highest levels of *MYC* expression and *MYC* amplification are found almost exclusively in the aggressive MYC-subgroup disease (Cho et al., 2011; Northcott et al., 2011). Thus, whereas *MYCN* may play a role in the pathogenesis of a variety of MBs, *MYC* may drive a specific aggressive subgroup of the disease. This may seem somewhat counterintuitive, because it is widely thought that the biochemical transcriptional functions of different MYC-family genes are similar.

Here, we assessed the role of MYC and MYCN in medulloblastoma development in the absence of TRP53.

RESULTS

Enforced Expression of *Myc* but Not *Mycn* in *Trp53*-Deficient Cerebellar Neuronal Progenitors Induces Aggressive MB

We showed previously that GNP-enriched cell isolates from the cerebella of postnatal day (P)6–P7 *Cdkn2c*$^{-/-}$, *Ptch1*$^{+/-}$ or *Cdkn2c*$^{-/-}$, *Trp53*$^{-/-}$ mice, but not from *Cdkn2c*$^{-/-}$ or wild-type mice, generate SHH-subgroup MBs when transduced with a retroviral vector expressing *Mycn* but not a control virus (Zindy et al., 2007). To test if *Myc* might similarly transform *Cdkn2c*$^{-/-}$, *Trp53*$^{-/-}$ GNPs, we isolated proliferating GNPs from *Cdkn2c*$^{-/-}$, *Trp53*$^{-/-}$, *Atoh1-GFP* mice, which are marked by co-expression of green fluorescent protein (GFP; Lumpkin et al., 2003). Enrichment of GNPs showed that, on average, we obtained 91.9% of GFP-positive (+) GNPs and 8.1% of GFP-negative (−) progenitor cells per preparation and found that the sorted GFP-expressing population contained 1.1% of GFP$^-$ cells, and, conversely, the GFP$^-$ population contained 1.7% of GFP$^+$ cells. We transduced these cells with viruses either encoding *Myc* and co-expressing red fluorescent protein (*RFP*) or expressing *Mycn* in lieu of *Myc*. Fluorescence-activated cell sorting (FACS) of *Myc*- and *Mycn*-transduced cells confirmed comparable infection efficiencies by the two retroviral vectors (45.9 ± 11.7% of GFP$^+$/RFP$^+$ for *Myc-RFP* and 51.6 ± 2.1% of GFP$^+$/RFP$^+$ for *Mycn-RFP*). Cells transduced with either *Myc* or *Mycn* (2×10^6 per mouse) were injected separately into the cerebral cortices of naïve recipient CD-1 *nu/nu* mice. *Myc*-transduced cells formed aggressive tumors that killed mice significantly faster than GNPs transduced with *Mycn* (median survival = 33 days for *Myc* vs. 48 days for *Mycn*, $p < 0.0001$, Figure 1A). Immunoblotting demonstrated significant levels of ectopic Myc or Mycn protein expression within the two tumor subsets (Figures S1A and S1B available online). *Myc*-derived tumors generated from P6–P7 cerebellar cells of either *Cdkn2c*$^{-/-}$, *Trp53*$^{-/-}$, or *Trp53*$^{-/-}$ mice occurred with similar latency (median survival = 39 days for *Cdkn2c*$^{-/-}$, *Trp53*$^{-/-}$ vs. 39 days for *Trp53*$^{-/-}$, $p = 0.7096$), indicating that the loss of *Cdkn2c* was not required for *Myc* expression to induce MB in the absence of *Trp53* (Figure S1C). Myc-tumors displayed a consistent morphology that was strikingly similar to human MBs of the MYC-subgroup (Figure 1B). Morphometric and terminal deoxynucleotidyl transferase dUTP nick end labeling (TUNEL) assays of mouse MBs revealed a much larger cell size and apoptotic rate in Myc-tumors than did mouse models of the WNT- (Gibson et al., 2010) or SHH-subgroups disease (Ptch-tumors; Uziel et al., 2005), which typically show a classic morphology (Figures 1B and 1C). Thus, Myc-induced mouse MBs resemble the human LC/A MB phenotype reported previously (McManamy et al., 2003), and *Myc* and *Mycn* drive distinct tumors that appear to recapitulate aggressive LC/A and classic forms of human MB, respectively.

Myc-engineered Murine MBs Have a Distinct Transcriptome that Mimics Human MYC-Subgroup Tumors

The decreased latency and LC/A morphology of *Myc*-generated tumors suggested that these were distinct from classic MBs induced by *Mycn*. We compared gene expression profiles of *Myc*-tumors with those of *Mycn*-tumors, as well as profiles generated from previously characterized mouse models of WNT- and SHH-subgroup MB (Gibson et al., 2010; Uziel et al., 2005). In addition, we compared these tumor profiles with those of FACS-sorted Atoh1-GFP-expressing GNPs obtained from the cerebellum of normal P6 mice lacking both Trp53 and p18^{Ink4c} protein expression [*Cdkn2c*$^{-/-}$, *Trp53*$^{-/-}$, *Atoh1-GFP*] mice (designated GNPs; Figure 2A). The transcriptome of Myc-tumors was distinct from those of the other mouse MBs (Figure 2A). Unsupervised hierarchical clustering co-segregated the gene expression profiles of mouse Mycn-tumors and those of mouse models of SHH-subgroup disease. In contrast, transcriptomes of Myc-tumors and the mouse WNT-subgroup model formed two separate clusters. The Mycn/SHH/GNP profiles

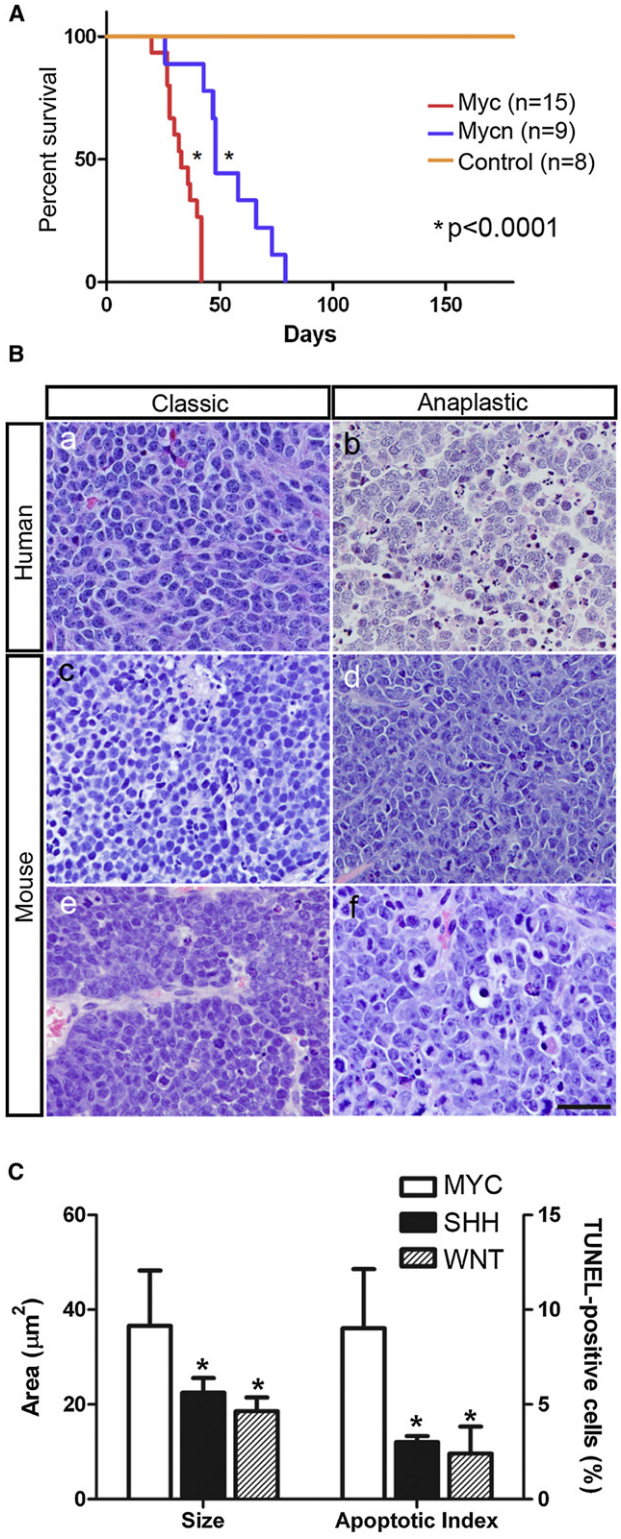

Figure 1. MBs Derived from Orthotopic Transplants in the Cortices of Naive Recipient Mice of Cerebellar Progenitors Overexpressing *Myc* and *Mycn*

(A) Kaplan-Meier survival curves of mice transplanted with cerebellar cells purified from [*Cdkn2c*$^{-/-}$, *Trp53*$^{-/-}$, *Atoh1-GFP*] mice infected with *Myc-RFP* (red line), *Mycn-RFP* (blue line), or *RFP* empty vector (orange line).

(B) Pathology of human and mouse MBs (H&E): (a) a human tumor with *MYCN* amplification and classic morphological features, and (b) a human anaplastic tumor with *MYC* amplification. Note the difference in nuclear pleomorphism between classic and anaplastic tumors. The anaplastic tumor also shows a paving stone-like pattern of cell molding and contains abundant apoptotic cells, a hallmark of this variant. Mycn-tumors with a classic morphology of round cells (c, e) contrast with Myc-tumors that show an anaplastic morphology with cell molding and abundant mitotic figures and apoptotic bodies (d, f). Scale bar = 50 μm.

(C) Myc-tumor cells are significantly larger and more likely to undergo apoptosis than are their SHH- and WNT-subgroups counterparts. Error bars indicate standard deviation. *p < 0.05 for SHH- and WNT-subgroup tumors compared to the MYC-subgroup. See also Figure S1.

were characterized by high expression of known members of the SHH pathway and signature genes of SHH-subgroup MB (Figure 2B). This observation was confirmed by quantitative RT-PCR (qRT-PCR), including analysis of *Atoh1*, *Gli1*, *Sfrp1*, and *Boc1* (Figures 2C and 2D). In contrast, *Myc* and *Npr3*, which are specifically expressed in the human MYC-subgroup (Northcott et al., 2011), were highly expressed in the mouse *Myc*-derived MBs (Figure 2B). Immunohistochemical analysis confirmed that Npr3 is expressed selectively in mouse MYC-subgroup MBs (Figure S2A). Myc-induced tumors also exhibited high levels of transcription of *Prom1* and *Lgr5* (Figure 2B), which are frequently expressed in stem-cell-like progenitor cells (Barker et al., 2007; Lee et al., 2005; Zhu et al., 2009). In addition, high expression of Nanog and Oct4 proteins, considered to be canonical markers of embryonic pluripotency (Silva and Smith, 2008), was observed in mouse MYC-subgroup and SHH-subgroup MBs (Figures S2B–S2P). On the other hand, putative markers of brain tumor stem cells (Rich, 2009) exhibited various expression levels among the three distinct tumor subgroups (Figure S2Q).

As a further test of the degree to which mouse Myc-derived tumors resemble the MYC-subgroup of human MB, we compared the expression of mouse genes with orthologs previously shown to specifically distinguish the human WNT-, SHH-, and MYC-subgroup tumors (Cho et al., 2011; Northcott et al., 2011; Thompson et al., 2006). Thirty-one of 52 orthologs (60%) that exhibited increased expression in the human MYC-subgroup were similarly upregulated in the mouse Myc-tumors (Figure 3A). Forty of 54 orthologs (74%) with increased expression in the human WNT-subgroup were similarly increased in the mouse WNT-tumors (Figure 3B). Thirty-one of 53 orthologs (58%) upregulated in the human SHH-subgroup were increased in the mouse Ptch-tumors (Figure 3C). Thus, mouse Myc-induced tumors express signature genes remarkably similar to those reported for human MYC-subgroup MB, whereas the mouse Mycn, Ptch, and Trp53 tumors resemble the human SHH-subgroup, and WNT mouse tumors recapitulate human WNT-subgroup MBs, as reported previously (Gibson et al., 2010). Furthermore, cross-species comparison of human and mouse MB transcriptomes (Johnson et al., 2010) revealed a statistically significant match between mouse and human MYC-subgroups (Figure S3A). Overall, 56% of 14,261 ortholog probe pairs showed agreement in gene expression (upregulation or downregulation) between the human MYC-subgroup and mouse Myc-tumors ($p = 0.009$ and $p = 0.079$ by permutation of the human and mouse data, respectively;

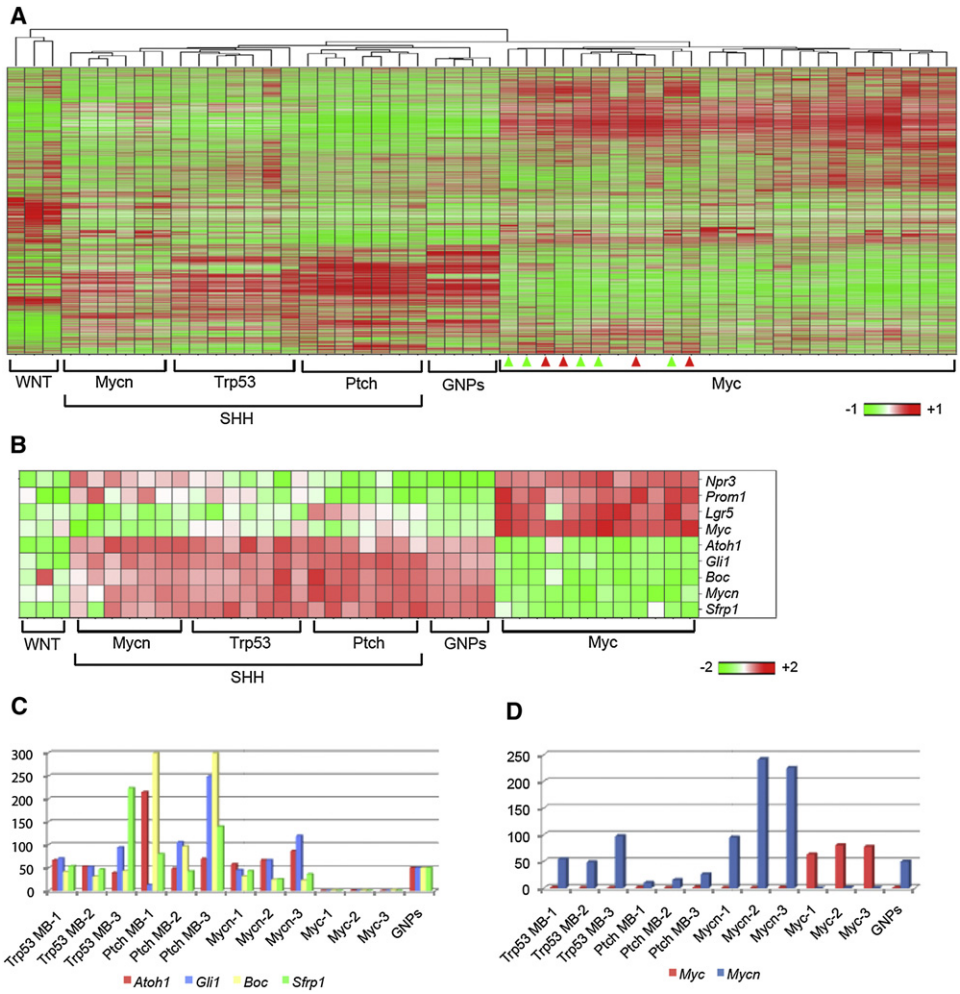

Figure 2. Comparative Molecular Analysis of Engineered Mouse MBs and GNPs

(A) Affymetrix gene chip analysis of mouse Myc- and Mycn-tumors, GNPs purified from the cerebellum of P6 [*Cdkn2c*$^{-/-}$, *Trp53*$^{-/-}$, *Atoh1-GFP*] mice, from spontaneous MBs of the SHH-subgroup from [*Cdkn2c*$^{-/-}$, *Trp53*$^{-/-}$, *Nestin-cre*] and [*Cdkn2c*$^{-/-}$, *Ptch1*$^{+/-}$] mice and from the mouse WNT-subgroup from [*Ctnnb1*$^{+/lox\ (ex3)}$; *Blbp-Cre*; *Trp53*$^{-/-}$] mice. Arrowheads indicate Myc-tumors from FACS-sorted GFP-positive (GFP^{+}; green) and GFP-negative (GFP^{-}; red) cerebellar cells.

(B) Heatmap of differentially regulated genes between Myc- and Mycn-mouse MBs and the SHH-subgroup MBs from the *Ptch1*$^{+/-}$ and *Trp53* null mice, the WNT-subgroup of tumors, and GNPs.

(C and D) Quantitative RT-PCR (QRT-PCR) analysis of *Atoh1, Gli1, Boc*, and *Sfrp1* (C) and *Myc* and *Mycn* (D) in *Myc*-engineered MBs (Myc-1,2,3) compared to spontaneous Trp53 and Ptch MBs, *Mycn*-engineered (Mycn-1,2,3) MBs, and GNPs. See also Figure S2.

Figure S3B). Together, these data confirm that the mouse Myc-tumors accurately model the transcriptome of human MYC-subgroup MB.

Probing the Origin of *Myc*-Engineered MBs

All MBs generated from neuronal progenitors purified from P7 cerebella of *Cdkn2c*$^{-/-}$, *Trp53*$^{-/-}$, *Atoh1-GFP* mice and infected with *Myc*-encoding retroviruses before cortical injection expressed vector-encoded RFP (Figures 1 and S1D). Mycn tumors consisted mainly of GFP^{+}/RFP^{+} cells (70.0 ± 8.20%, n = 7; Figure S1E). Surprisingly, *Myc*-induced tumors expressed little or no GFP (17.2 ± 3.67%, n = 14; Figure S1E), suggesting that these tumors arise from a small fraction (~5%) of GFP^{-} cells in the GNP-enriched isolates or from GFP^{+} GNP progenitors that subsequently silence Atoh1-GFP expression during tumor formation.

To more rigorously characterize the source of mouse MYC-MBs, we further profiled our cell isolates. Comparison of gene expression profiles between GFP^{+}, GFP^{-} populations and *Myc*-engineered MBs revealed that MYC-subgroup medulloblastoma most closely matched that of GFP-negative cells (Figure S4A); however, not all genes, including *Lgr5* and *Npr3,* were expressed in the GFP-negative sorted cell population (Figure S4B). As a first step in understanding which cell population might generate MYC-subgroup MBs, we FACS-sorted GFP-positive and GFP-negative progenitor cells. These separate fractions were then transduced with *Myc*-encoding retroviruses at an efficiency of ~30%, and 5 × 10^{4} cells from each transduced fraction were

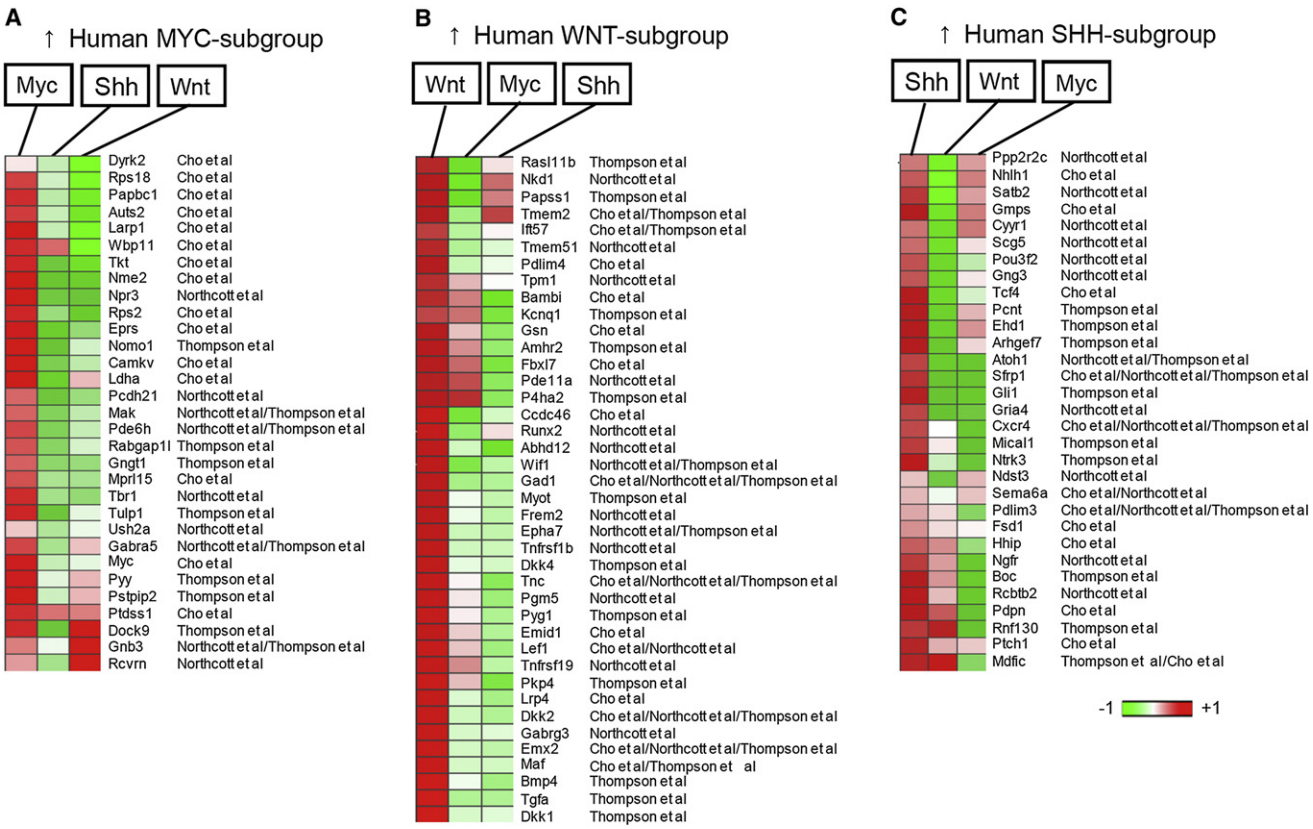

Figure 3. Comparison of the Gene Expression Signature of Human MYC-, SHH-, and WNT-Subgroup MB with that of Mouse MBs Reveals Three Representative Murine Models of the Human Disease

Signature genes that specifically distinguish the human WNT-, SHH-, and MYC-subgroup tumors by their broad subgroup overexpression relative to the others were compiled from three recent publications on subgroups of MB (Cho et al., 2011; Northcott et al., 2011; Thompson et al., 2006). 52 signature genes relatively overexpressed by the human MYC-subgroup, 54 by the human WNT-subgroup, and 53 by the human SHH-subgroup were found to have corresponding mouse orthologs on the Affymetrix 430v2 chip. Shown here are representative heat maps columns which compare mean average expression of the orthologs in the three mouse medulloblastoma models (Myc, Shh, and Wnt). Red indicates a log scale relative increase of expression, whereas green signifies a log scale relative decrease of expression. The ortholog name and the corresponding first author of the study from which the signature gene was described are listed in the columns immediately to the right of the heat map.

(A) Thirty-one of 52 orthologs (60%) with increased expression in the human MYC-medulloblastoma subgroup and in the mouse Myc-tumors.

(B) Forty of 54 orthologs (74%) with increased expression in the human WNT-subgroup and in the mouse WNT-tumors.

(C) Thirty-one of 53 orthologs (58%) with increased expression in the human SHH-subgroup and mouse Ptch-tumors. See also Figure S3.

then separately implanted into the cortices of recipient mice. Both *Myc*-transduced population generated tumors in the cortex of naïve recipient animals (Table 1). Histopathological analysis of tumors revealed that all medulloblastomas derived from GFP^+ FACS-sorted cells infected with *Myc*-encoding viruses (5/8) showed LC/A characteristics (Table 1 and Figure S4C). In contrast, tumors occurring after transplants of GFP-negative cells infected with *Myc*-expressing retroviruses included two T-cell lymphomas (2/8), as well as a range of CNS embryonal tumors—high-grade neuroepithelial tumor with dominant PNET and focal glial phenotype (3/8) and MBs with LC/A features (3/8; Table 1). All LC/A MBs expressed low levels of *Atoh1* when compared to that of normal GNPs percoll-purified from the cerebella of P7 wild-type mice (Figure S4D). Comparative gene expression analysis showed that the MYC-subgroup MBs derived from *Myc*-transduced FACS sorted GFP-positive and GFP-negative cerebellar cell populations had similar gene profiles as do Myc-tumors derived from unsorted cerebellar cells (Figure 2A). These observations suggest that both GFP^+ and GFP^- populations contain cells that can form MYC-subgroup MBs.

Myc-Engineered MBs Contain Numerous Tumor-Propagating Cells with High Proliferative Potential

Human MYC-type MBs are the most aggressive of all subgroups (Cho et al., 2011; Northcott et al., 2011), and consistent with clinical data, mouse Myc-induced tumors developed faster than did Mycn-MBs (Figure 1A). One possible feature of MYC tumors that could explain their aggressiveness is that MYC-subgroup MBs contain a greater fraction of tumor-propagating cells than do tumors of other subgroups. To estimate the numbers of cells capable of initiating MBs, cells were purified from mouse MBs of the SHH- and MYC-subgroups, and different numbers of tumor cells were injected into the cortices of recipient nude mice (Figure 4A). Limited dilution experiments revealed that

Table 1. Orthotopic Transplants of FACS sorted Cerebellar Progenitor Cells before Infection with *Myc*-Encoding Retroviruses

Myc-Infected FACS-Sorted Population	Transplanted Cells (Number)	Tumor Latency (Days)	Phenotype
GFP^+ (n = 8)	5×10^4	52, 55, 98, 113, 75	LC/A, MYC-subgroup
GFP^- (n = 8)		34, 37	T cell lymphoma
	5×10^4	51, 53, 69	High-grade neuroepithelial tumor with dominant PNET and focal glial phenotype
		60, 68, 60	LC/A, MYC-subgroup

Neuronal progenitors were purified from the cerebella of postnatal day P7 *Cdkn2c*$^{-/-}$; *Trp53*$^{-/-}$; *Atoh1-GFP* mice and sorted for GFP-positive and GFP-negative cell populations. Sorted cells were infected with vectors co-expressing both *Myc* and *RFP*, and 5×10^4 cells were transplanted into the cortices of naïve recipient animals. Data were obtained from three independent experiments. Tumor latency represents the time at which mice become moribund (median survival = 105.5 days for GFP-positive population and 56.5 days for GFP-negative population). See also Figure S4.

equal to more than 2×10^5 purified SHH-subgroup tumor cells were required for secondary tumor formation (Figure S5), consistent with previous reports (Read et al., 2009). Unlike SHH-subgroup MB cells, only 1×10^2 Myc-induced tumor cells were required to generate secondary tumors (5/5; Figure 4A). Histological analysis confirmed that secondary tumors shared similar immunohistological characteristics with the parental primary tumor (Figures 4B–4K).

CD133/Prom1-positive tumor-propagating cells from human MBs expand in vitro to form "neurosphere" colonies when plated under conditions that prevent their attachment to the culture dish (Singh et al., 2004). Given that mouse MYC-subgroup tumors upregulated *Prom1*, we tested whether these tumor cells could similarly form neurospheres. Purified cells from Myc-tumors were plated on an ultra-low attachment dish at a density of 5×10^4 cells/ml in culture medium supplemented at 3-day intervals with basic fibroblast growth factor (FGF) and epidermal growth factor (EGF). One week later, spheres were harvested, dissociated with trypsin, and the total number of cells per plate was enumerated. Dissociated cells were replated at the same initial density, cultured under the same conditions, and sequentially passaged multiple times. Six to seven days after their first plating, single RFP-positive Myc-derived tumor cells generated macroscopic red colonies (Figure 5A), the overall numbers of which had increased more than 20-fold (Figure 5B, passage 1). Thus, on average, sphere-forming cells underwent 5–6 population doublings in the first 7-day period. More cells were recovered at passages 2 and 3, after which the doubling time of the population slowed down; however, a consistent proliferative rate approximately equal to 4 population doublings in the succeeding 7-day intervals was maintained from passages 5 to 10 (Figure 5B). In stark contrast, spheres derived from canonical SHH-subgroup MBs that arose in *Cdkn2c*$^{-/-}$, *Ptch1*$^{+/-}$ mice could not be serially passaged at all under the same culture conditions (Figure S6). Immunohistochemical analysis (Figure 5C) and qRT-PCR (Figure 5D) revealed that neurospheres from Myc-induced MBs expressed several markers identified in stem/progenitor cells, including Nanog, Oct4, Sox2, and Lgr5, as well as Nestin and Npr3 (Figure 5C).

To examine whether tumor spheres could be transplanted and would recapitulate primary Myc-induced MBs, we injected spheres at passages 2 and 6 into the cortices of recipient mice. Interestingly, 2×10^5 cells formed tumors with a similar latency as the secondary MBs generated from cells purified from *Myc*-engineered tumors (7/7, median latency = 22 days; Figure 6A). Primary and secondary tumors shared the same pathology and expressed similar immunohistochemical markers (Figure 6B). Gene profiling of primary and secondary MBs confirmed that the tumors were distinct from the SHH-subgroup tumors used as a control (Figure 6C). Thus, tumor spheres recapitulate MYC- subgroup MBs after transplantation.

Myc-Engineered MB Cells Are Resistant to SHH Signaling Inhibitors

Smoothened inhibitors, including cyclopamine and HhAntag, inhibit the proliferation and induce the differentiation of SHH-subgroup MB in vitro and in vivo (Berman et al., 2002; Romer et al., 2004). Similarly, BMP4 antagonizes SHH signaling, induces the neuronal differentiation of GNPs (Rios et al., 2004), extinguishes protein Atoh1 expression, and inhibits the proliferation of MBs of the SHH-subgroup (Zhao et al., 2008). Because human MYC-subgroup MBs lack an active SHH gene expression signature and do not contain activating mutations in SHH pathway genes, we reasoned that mouse MYC-subgroup tumors might resist smoothened antagonists. Purified GNPs from cerebella of P7 wild-type mice, from MYC-subgroup MB, and from a SHH-subgroup MB derived from *Cdkn2c*$^{-/-}$, *Trp53*$^{Fl/Fl}$, *Nestin-Cre* mice were cultured for 3 days, either in the presence of cyclopamine, BMP4, or a vehicle control. Cells were then labeled with BrdU and analyzed by FACS with an antibody to BrdU. Cyclopamine or BMP4 reduced the S phase fraction of *Cdkn2c*$^{-/-}$, *Trp53*$^{Fl/Fl}$, *Nestin-Cre* "primary" tumor cells by 35% to 85% (Figure 7A). In contrast, tumor cells isolated from 3 independently derived mouse MYC-subgroup tumors were insensitive to cyclopamine or BMP4 treatment (Figure 7A), consistent with the finding that MYC-tumors were associated with low expression of SHH signature genes (Figure 7B). Similarly, we saw no inhibition of proliferation of neurospheres from MYC-tumors plated in the constant presence of SHH signaling inhibitors in the culture medium for 2 weeks (Figure 7C).

DISCUSSION

Enforced expression of *Myc*, but not *Mycn*, in concert with the loss of *Trp53* in GNP-enriched mouse cerebellar progenitor cells gives rise to tumors that recapitulate the most aggressive form of human MB. These tumors exhibited neither of the characteristic gene expression signatures previously ascribed to the SHH- or

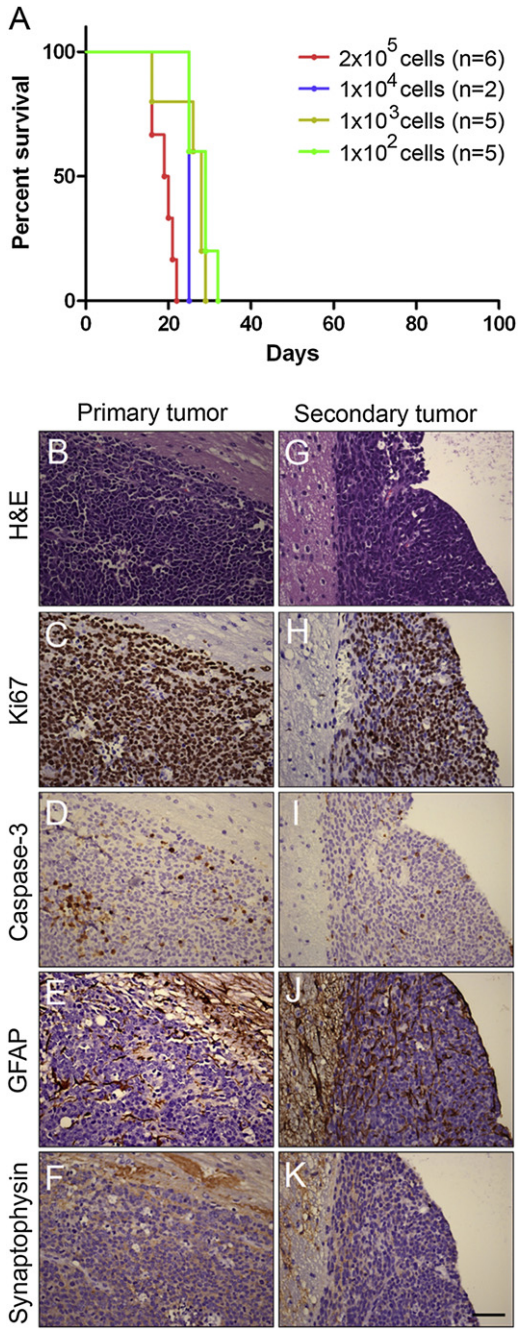

Figure 4. Mouse MYC-Subgroup MBs before and after Orthotopic Transplants

(A) Kaplan-Meier survival curve of mice subjected to orthotopic cranial injection of decreasing number of Myc- primary tumor cells.

(B–K) Sections of tumors were immunostained with H&E (B and G), Ki67, a marker of proliferating cells (C and H), cleaved Caspase-3, a marker of apoptosis (D and I), GFAP, that marks glial and neural progenitor cells (E and J), and synaptophysin that characterizes mature neurons (F and K). Scale bar = 50 μm. See also Figure S5.

WNT-subgroups of the disease (Cho et al., 2011; Northcott et al., 2011; Thompson et al., 2006). Instead, multitiered analysis of data comparing the murine tumors with the human MYC-subgroup revealed convincing similarities in histology, clinical behavior, and gene expression between the tumors of both species.

Marker proteins, including Prom1, Lgr5, Oct4 and Nanog, found either in embryonic or adult tissue stem cells, as well as in some "cancer stem cells," were highly expressed as part of the defining gene expression signature of *Myc*-engineered tumors. Prom1 is a marker of tumor-initiating cells in many cancers (Curley et al., 2009; Reya et al., 2001; Singh et al., 2004; Todaro et al., 2010), and Lgr5 is expressed in mitotically dividing stem cells within the colon and intestinal crypts but not in their proliferating transient amplifying progeny (Barker et al., 2007; Zhu et al., 2009). Oct4 and Nanog are considered markers of pluripotency; although distinct from the "MYC expression module" (Kim et al., 2010), they can collaborate with MYC in reprogramming somatic cells to induced pluripotent stem cells (Takahashi and Yamanaka, 2006). Like those cells with stem cell characteristics, whose frequencies correlate with poor prognosis in other cancers (Ben-Porath et al., 2008), cells from mouse MYC-subgroup MBs could be sequentially and continuously propagated as cultured neurospheres through many ex vivo passages. These cells retained tumor-propagating potential after transplantation into the cortices of recipient mice and re-induced MBs with the same robust efficiency and defining cardinal features as the primary MYC-subgroup MBs from which they were derived. In contrast, tumor cells explanted from MBs of the SHH-subgroup tend to undergo spontaneous differentiation in culture, and neurospheres generated from these tumors rapidly lose their self-renewal capacity when sequentially passaged (Read et al., 2009; Figure S5). Given that standard front line therapies fail in children with MYC-subgroup MBs and such tumors in the mouse are unaffected by SHH inhibitors now being incorporated into human clinical trials, the ability to maintain tumor-propagating cells in cultures from mouse MYC-subgroup MBs may prove useful in establishing a platform for identifying therapeutic drugs.

The generation of an entirely unique subgroup of MB in the mouse after *Myc* transduction into *Trp53*-deficient GNPs (irrespective of *Cdkn2c* loss) was unexpected. In fact, upon embarking on these experiments, a reasonable hypothesis might have been that ectopically enforced overexpression of *Myc* would have had the same effect as overexpression of *Mycn*, given that Myc-family proteins bind to the same canonical DNA consensus sequences (Grandori and Eisenman, 1997) and interact with similar dimerization partners, co-activators, and corepressors (Blackwood and Eisenman, 1991; Grandori et al., 2000). Indeed, despite the fact that *Mycn* and *Myc* genes are differentially expressed in the hindbrain (Zindy et al., 2006) and that Mycn, but not Myc, is a target of SHH signaling (Kenney et al., 2003), genetic experiments showed that *Mycn* can functionally replace *Myc* in mouse development, proliferation, and differentiation (Malynn et al., 2000), implying many interchangeable functions.

The gene expression pattern of the human SHH-subgroup MB resembles that of GNP cells (Lee et al., 2003) and that of the WNT-subgroup MB resembles cells derived from the dorsal brainstem (Gibson et al., 2010), but the gene expression pattern of the MYC-subgroup of MB, either in mouse or humans, is quite distinct. This suggests that the latter tumors might arise from a class of MYC-responsive progenitor cells that differ from those

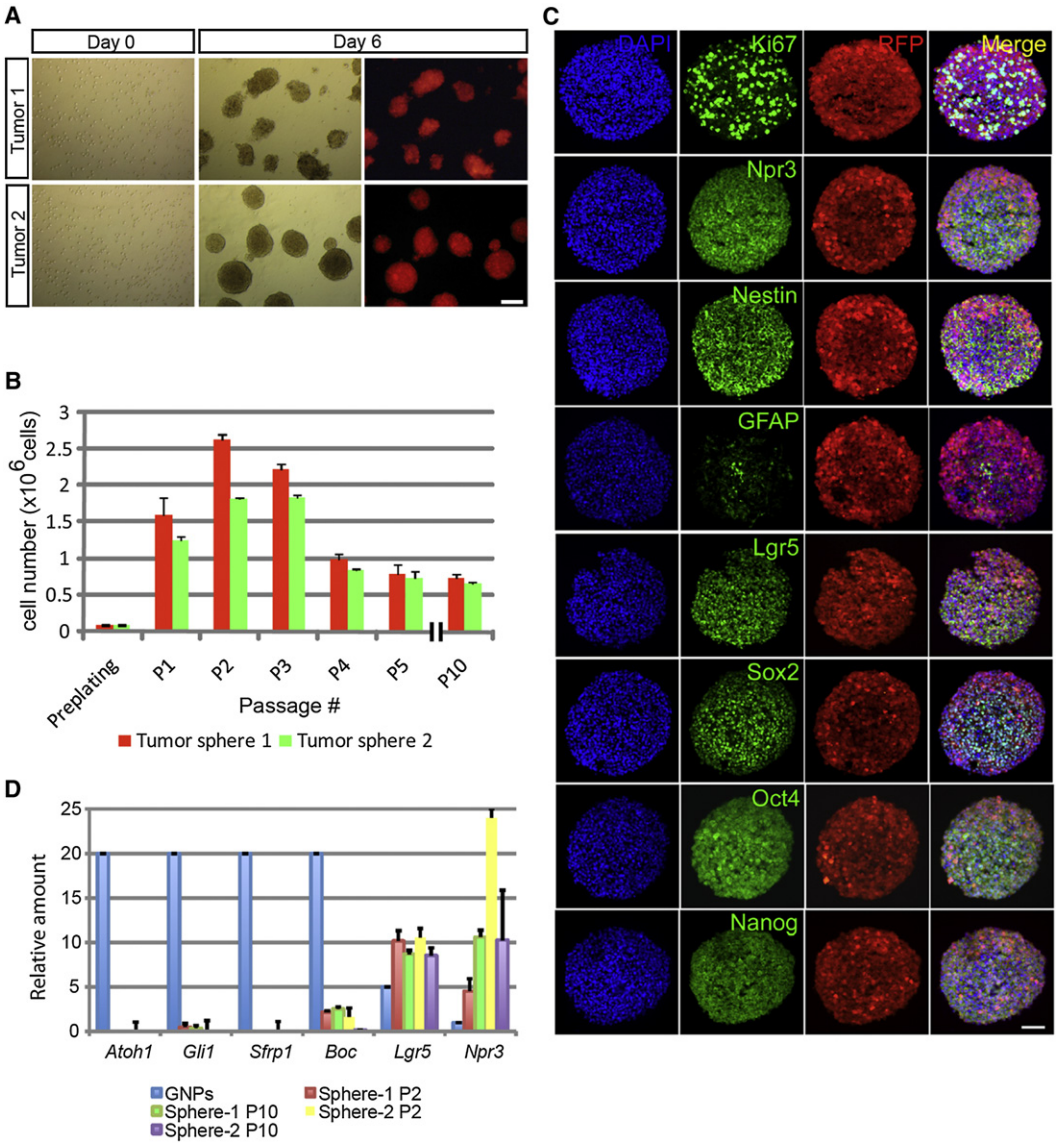

Figure 5. Myc-Induced Tumor Cells Grow as Neurospheres In Vitro

(A) Tumor cells from mouse MYC-subgroup MBs form red spheres by day 6 after plating. Scale bar = 200 μm.

(B) Spheres can be passaged continuously; here shown up to passage 10 with the cell number increasing up to 25-fold.

(C) Immunostaining of tumor spheres with antibodies against Ki67, Npr3, Nestin, Sox2, Oct4, Nanog, Lgr5, and GFAP. Scale bar = 50 μm.

(D) Spheres share a similar molecular signature (lower levels of SHH signature genes and higher levels of *Lgr5* and *Npr3*) than that of GNPs after several passages up to passage 10. Data are represented as the mean ± SD. See also Figure S6.

that give rise to the other MB subgroups. Notably, although previous models of mouse MB generated by targeting cerebellar GNPs invariably yielded tumors of the SHH-subgroup, regardless of many different genetic perturbations used to initiate tumorigenesis (Wu et al., 2011), the more recent derivation of a WNT-subgroup mouse model stemmed from observations that a different group of progenitor cells expressed in the dorsal brain stem, and not cerebellar GNPs, were the most sensitive to constitutive activation of the WNT signaling pathway (Gibson et al., 2010). Therefore, one possibility is that target cells most sensitive to Myc overexpression had contaminated the highly purified Atoh1-GFP-expressing GNP population into which the *Myc-RFP* vector was introduced. Alternatively, enforced *Myc* expression in the context of *Trp53* loss may have significantly altered the transcriptional program of GNPs, resulting in their transdifferentiation, loss of canonical GNP markers, and the emergence of distinctly different phenotypic features. Either scenario would account for the observation that RFP-expressing MYC-subgroup MBs no longer expressed Atoh1-GFP. By analogy to the strategy for modeling WNT-subgroup MBs (Gibson et al., 2010), the identification of the cell of origin of MYC-subgroup tumors will likely require the systematic generation of genetically engineered animals in which *Myc* expression is conditionally regulated within different cell lineages.

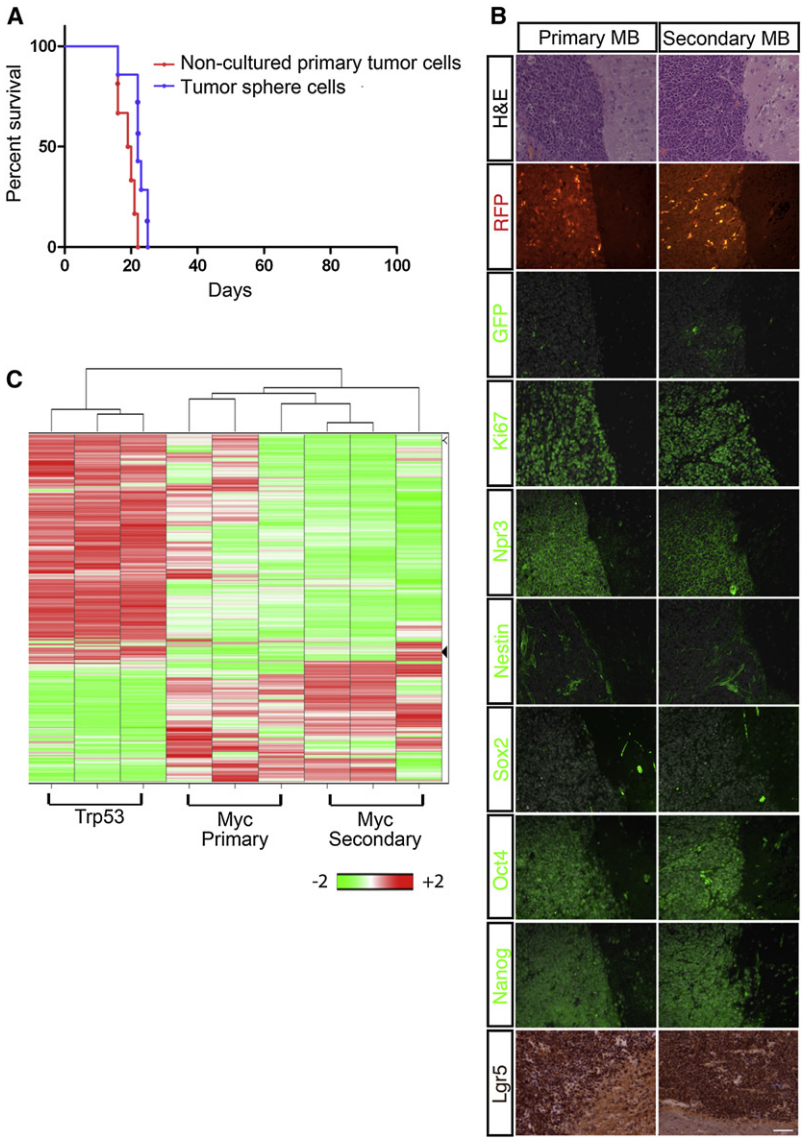

Figure 6. Tumor Sphere Cells Contain Tumor-Propagating Cells

(A) *Myc*-engineered MBs form after transplant of purified tumor cells or tumor sphere cells at passage 2 (2×10^5 cells) into the cortices of recipient mice.

(B) Comparison of the expression of RFP, GFP, Ki67, Npr3, Nestin, Sox2, Oct4, Nanog, and Lgr5 by immunohistochemistry between primary MB (Primary MB) and those induced after transplant of spheres (Secondary MB). Scale bar = 50 μm.

(C) Comparison of gene signature among Trp53 tumors, Myc-primary tumors, and Myc-secondary tumors.

Recent studies have more clearly identified the subgroup of human MBs that feature high *MYC* expression and/or amplification and carry a dismal prognosis (Cho et al., 2011; Ellison et al., 2011b; Northcott et al., 2011). Both amplification and overexpression of *MYC* or *MYCN* have been associated with poor prognosis in human MB (Pfister et al., 2009). However, in a large cohort of children studied in the SIOP/PNET3 clinical trial, Ellison et al. (2011b) recently concluded that amplification of *MYC*, rather than *MYCN*, is associated with the poorest outcome. In agreement with the latter findings, Myc-induced mouse MBs were more anaplastic and aggressive than were their Mycn-induced counterparts, contained a several log-fold higher fraction of tumor-propagating cells, and initiated tumors after a significantly shorter latency period.

Whereas our finding that *Mycn* overexpression results in MBs of the SHH-subgroup seems contradictory to the finding published in a recent study by Swartling et al. (2010), which ascribes *Mycn* overexpression to the production of a variety of MBs, we feel that there are distinctions in the two models that may explain this discrepancy. The Swartling model links *Mycn* to a *Glt-1* promoter. *Glt-1* is a gene that is not widely expressed by cells in the external granule layer (EGL) of the cerebellum, and it is likely that, via *Glt-1*, *Mycn* is influencing a developing cerebellar cell pool that is distinct from that of the EGL. On the contrary, in our study *Mycn* is transfected into a highly concentrated pool of GNP cells. It stands to reason that the introduction of a SHH pathway target member, like *Mycn* into GNP/EGL cells, which are particularly sensitive to SHH stimulated growth, may favor the induction of SHH-subgroup MB. On the other hand, MYC—probably because it is not a direct target of the SHH pathway—appears to have a very unique and specific effect when transduced into a similar pool of cerebellar precursor cells.

Mutations of the *TP53* gene are found in human LC/A MBs together with *MYC* amplification (Aldosari et al., 2002; Frank et al., 2004; Pfister et al., 2009). Although *TP53* is frequently disrupted in LC/A MBs, its loss of function is observed only infrequently across other subgroups (Pfaff et al., 2010; Thompson et al., 2006). Under the conditions used in our mouse modeling experiments, concurrent deregulation of both *Myc* and *Trp53* was required to induce MYC-subgroup tumors, whereas neither was effective alone. The genetic interaction between *MYC* and *TP53* is known to be important in many different cancers. Whereas *Trp*53 represses *Myc* expression transcriptionally, miss-regulation of *Myc* abrogates *Trp*53-mediated cell cycle arrest through the repression of inhibitors of CDKs (Hoffman and Liebermann, 2008). Overexpression of *Myc* also induces *Trp*53-dependent apoptosis (Hermeking and Eick, 1994; Wagner et al., 1994), but when accompanied by either *Trp*53 mutation or bi-allelic *Arf* deletion, *Myc* can readily generate immortalized tumor cells (Eischen et al., 1999; Hemann et al., 2005; Zindy et al., 1998).

Sublethal ionizing irradiation of *Trp53* null mice at P5–P7 is sufficient to induce MBs of the SHH-subgroup with very high penetrance, implying that in this setting, the primary function of Trp53 is to eliminate rapidly proliferating GNPs that have sustained DNA damage (Uziel et al., 2005). Inactivation of *Trp53*

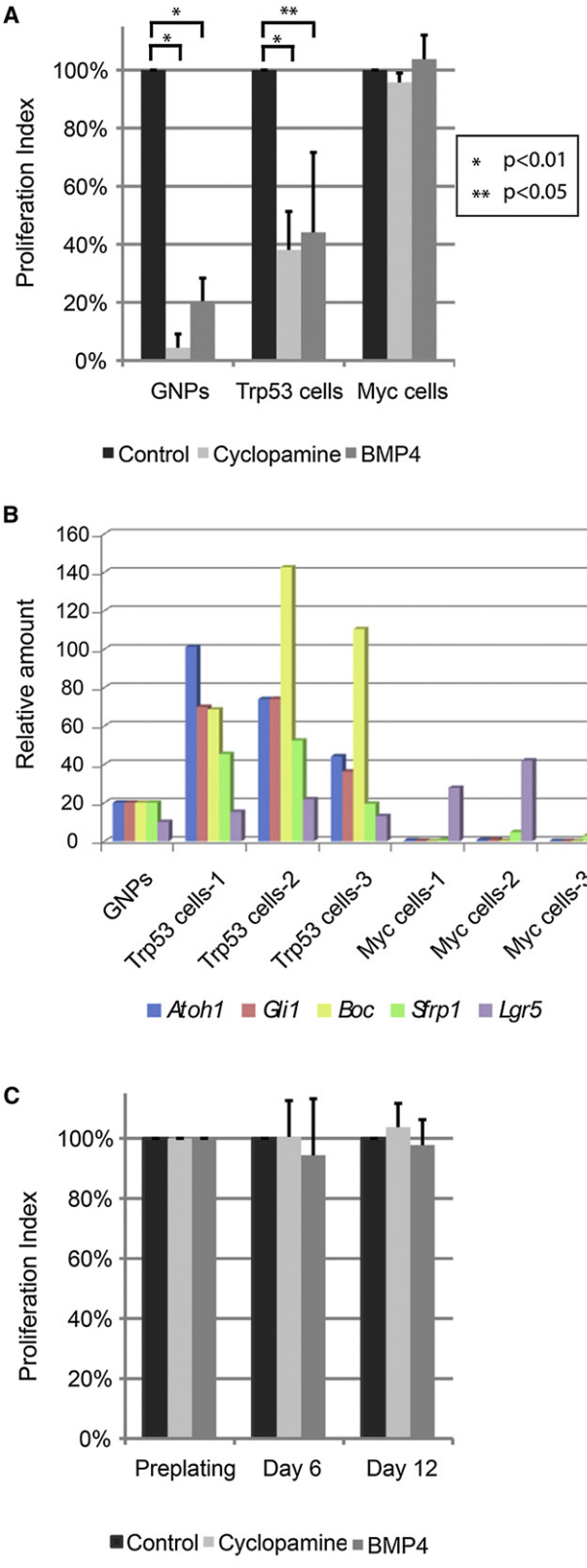

Figure 7. Myc-Tumor Cells Are Resistant to SHH Signaling Inhibitors

(A) GNPs purified from the cerebellum from 7-day-old pups and purified tumor cells were grown in serum-free medium in the absence (Control, black square) or the presence of cyclopamine (light gray square) or BMP4 (dark gray square). Proliferation was assessed by FACS by calculating the percent of BrdU positive cells. Proliferation index was defined as the ratio of the percentage of BrdU-incorporated cells with SHH signaling antagonists to that of control.

(B) GNPs and tumor cells were analyzed by qRT-PCR for specific gene expression to validate the expression of genes in the SHH signaling pathway.

(C) Treatment of MYC-tumor sphere cells with or without SHH signaling antagonists under neurosphere culture conditions. Proliferation index represents the ratio of cell number of cultured neurosphere cells with SHH signaling antagonists to that of control, 6 and 12 days after plating. Data in graphs A and C represent the mean ± SD.

similarly accelerates MB formation in *Ptch1* heterozygous mice, a context in which *Arf* deletion has no such effect (Wetmore et al., 2001). Although *Arf* is induced by high-signaling thresholds conveyed by constitutively activated oncogenes, including Myc (Zindy et al., 1998), *Arf* is not induced by acute DNA damage (Kamijo et al., 1997). Moreover, Atoh1-expressing, proliferating GNPs normally express relatively high levels of Bmi1, a polycomb protein suppressor of the *Ink4a/Arf* locus (Bruggeman et al., 2005). If the cell of origin of Myc-induced tumors is not an Atoh1-expressing GNP, this begs the question of whether *Arf* null mice, like those lacking *Trp53*, might be predisposed to MYC-subgroup MB formation. Conceivably, other mutations in the *Trp53* signaling network might also substitute for inactivation of *Trp53* itself. Next-generation sequencing and comprehensive analysis of the methylome of primary MYC-subgroup human MBs should shed light on this issue.

In summary, the generation of a mouse model of MYC-subgroup MB is of particular importance, because it mimics the most aggressive subgroup of human MBs that remain the least responsive to therapy (Ellison et al., 2011b). The model provides an opportunity to further explore the identity of the progenitor cells from which these tumors arise and screen for molecules that may offer improved therapeutic impact.

EXPERIMENTAL PROCEDURES

A detailed description of the Experimental Procedures utilized in this work can be found in the Supplemental Experimental Procedures (available online).

Mouse Strains and Animal Husbandry

Cdkn2c$^{-/-}$, *Trp53*$^{-/-}$, *Atoh1-GFP* mice were generated by breeding *Cdkn2c*$^{-/-}$; *Trp53*$^{-/-}$ animals (Uziel et al., 2005) with *Atoh1-GFP* transgenic mice (Lumpkin et al., 2003). Other mice used in this study were *Cdkn2c*$^{-/-}$; *Ptch1*$^{+/-}$ (Uziel et al., 2005), *Cdkn2c*$^{-/-}$; *Trp53*$^{Fl/Fl}$; *Nestin-Cre*, and *CTNNB1*$^{+/lox\ (ex3)}$; *BLBP-Cre*; *Trp53*$^{Fl/Fl}$ (Gibson et al., 2010). All animal work was performed under established guidelines and supervision by the St. Jude Children's Research Hospital's Institutional Animal Care and Use Committee, as required by the United States Animal Welfare Act and the National Institutes of Health's policy to ensure proper care and use of laboratory animals for research.

GNP Culture, Retrovirus Production, and Infection

Purification of GNPs and other progenitor populations, retrovirus production, infections, and orthotopic transplants were performed as previously described (Ayrault et al., 2010). Mouse stem cell virus (MSCV)-based retroviruses encode the red fluorescent protein (*RFP*) in cis expressed from an internal ribosomal entry site. These viruses either express RFP alone or co-express mouse *Myc* or *Mycn* cDNA inserted downstream of the MSCV-LTR. Infection efficiency was analyzed using FACS for RFP and GFP expression. In some experiments, 2 days after plating, infected GNPs were harvested and transplanted into the cerebella or cortices of CD-1 *nu/nu* mice (Charles River Laboratories, Wilmington, MA, USA). In other experiments, GNP-enriched cerebellar cells

were sorted by FACS based on GFP expression immediately after purification. GFP^+ and GFP^- populations were independently infected with *Myc*-carrying retroviruses, and 5×10^4 infected cells from each population were transplanted into the cortices of mice 2 days after infection.

Orthotopic Transplants

Transplantation of infected GNP-enriched cerebellar cells into the cortices or cerebellum of nude recipient mice was performed essentially as described previously (Ayrault et al., 2010). After transplant of virus-infected progenitor cells, mice were examined daily for symptoms of sickness (doming of the head or ataxia or reduced activity). In some instances, purified MB cells or cultured tumor sphere cells from MYC-tumors were injected back into the cortices of naïve *nu/nu* recipient animals.

Tumor Cell Culture and BrdU Analysis

We analyzed progenitors purified from P7 wild-type mice and tumor cells from three independently derived *Myc*-engineered MBs and MBs arising spontaneously in *Cdkn2c*$^{-/-}$; *Trp53*$^{Fl/Fl}$; *Nestin-Cre* mice. Purified GNPs and tumor cells were plated at 8×10^5 cells/well on a Matrigel-coated 24-well plate and grown as previously described (Zhao et al., 2008). GNPs were treated with SHH, whereas tumor cells were not. Both cell populations were cultured in the presence or absence of SHH signaling inhibitors, 2.5 μM cyclopamine (LC Laboratories, Woburn, MA, USA), or 100 ng/ml BMP4 (R&D Systems). The medium was changed every 24 hr. Three days after initiation of culture, BrdU was added to the culture medium at a final concentration of 10 μM, and cells were harvested 2.5 hr later. Cells that incorporated BrdU were stained with an anti-BrdU antibody using a BrdU-APC flow kit (BD Bioscience, San Jose, CA, USA) and analyzed by FACS.

Histopathology, Immunohistochemistry, and Immunoblotting

For histopathology, samples of murine MBs (three separate tumors for each genotype) were formalin-fixed, paraffin-embedded, and sectioned at 5 μm thickness. For each sample, a section was stained using a standard hematoxylin and eosin (H&E) protocol; a second section was stained for apoptotic cells, using the ApopTag kit (Millipore, Billerica, MA, USA) with peroxidase detection of TUNEL labeling. Representative images of each sample/stain combination were captured (under oil immersion at 40× original magnification) and analyzed using Axiovision software (Carl Zeiss Microscopy, Thornwood, NY, USA). A single observer scored each tumor for apoptotic index (percentage of positive cells following ApopTag labeling) and nuclear area as previously described (McManamy et al., 2003).

For immunoblotting, purified GNPs from the cerebellum of P7 wild-type mice or *Myc*- and *Mycn*-engineered MB cells were lysed and proteins subjected to immunoblotting as described previously (Zindy et al., 2007).

Procedures and antibodies used for immunohistochemistry and antibodies for immunoblotting are provided in the Supplemental Experimental Procedures.

Affymetrix Microarray Analysis

RNA from GNPs or tumor cells were subjected to hybridization using Affymetrix Mouse Genechips 430 (version 2; e.g., Figures 2 and 3). For comparative gene expression analysis between primary and secondary *Myc*-engineered tumors, we used Affymetrix Mouse Genechips HT430PM (e.g., Figure 7C). Microarray results were validated by qRT-PCR using PCR primers shown in the Supplemental Experimental Procedures.

Neurosphere Assays

Tumor cells were cultured under conditions described previously (Taylor et al., 2005). Briefly, cells from *Myc*-engineered tumors were purified and plated on an ultra-low attachment dish at 5×10^4 cells/ml or 1×10^5 cells/well per 6-well plate. Human recombinant basic FGF and EGF (Peprotech, Rocky Hill, NJ, USA) were added into the culture medium every 3 days. One week later, tumor spheres were harvested, pooled, and dissociated with trypsin (Invitrogen, Grand Island, NY, USA), and total cell numbers were determined. In parallel, 1×10^5 of the dissociated cells were plated again and cultured under the same conditions. Total RNA was extracted from the reminder of the cultured cells followed by qRT-PCR analysis of selected RNAs. To test the role of SHH-antagonists, *Myc*-engineered tumor cells were cultured in the presence of 2.5 μM cyclopamine or 100 ng/ml BMP4.

ACCESSION NUMBERS

Affymetrix data for mouse MBs using 430V2 and HT430PM chips can be found in the GenBank database numbers GSE33199 and GSE33200, respectively.

SUPPLEMENTAL INFORMATION

Supplemental Information includes six figures and Supplemental Experimental Procedures and can be found with this article online at doi:10.1016/j.ccr.2011.12.023.

ACKNOWLEDGMENTS

We thank Dr. Robert Eisenman for helpful suggestions; Dr. Charles J. Sherr for editing of the manuscript; Dr. Frederique Zindy for mice; Shelly Wilkerson, Sarah Gayso, and Jennifer Craig for excellent technical assistance; John Morris for Affymetrix microarrays; Drs. Richard Ashmun and Ann-Marie Hamilton-Easton for FACS analysis; Dr. Chris Calabrese, John Killmar, and Melissa Johnson for orthotopic transplants; and Pamela Johnson and Dorothy Bush for immunohistochemistry of tumor tissues. This work was funded in part by the National Institutes of Health (grant CA-096832 to M.F.R. and CA-21765 to R.J.G. and M.F.R.), the American Brain Tumor Association (T.U.), the Mochida Foundation (D.K.), the Anderson fellowship (D.K.), and the American Lebanese Syrian Associated Charities of St. Jude Children's Research Hospital.

Received: July 8, 2011
Revised: November 2, 2011
Accepted: December 20, 2011
Published: February 13, 2012

REFERENCES

Aldosari, N., Bigner, S.H., Burger, P.C., Becker, L., Kepner, J.L., Friedman, H.S., and McLendon, R.E. (2002). MYCC and MYCN oncogene amplification in medulloblastoma. A fluorescence in situ hybridization study on paraffin sections from the Children's Oncology Group. Arch. Pathol. Lab. Med. *126*, 540–544.

Ayrault, O., Zhao, H., Zindy, F., Qu, C., Sherr, C.J., and Roussel, M.F. (2010). Atoh1 inhibits neuronal differentiation and collaborates with Gli1 to generate medulloblastoma-initiating cells. Cancer Res. *70*, 5618–5627.

Barker, N., van Es, J.H., Kuipers, J., Kujala, P., van den Born, M., Cozijnsen, M., Haegebarth, A., Korving, J., Begthel, H., Peters, P.J., and Clevers, H. (2007). Identification of stem cells in small intestine and colon by marker gene Lgr5. Nature *449*, 1003–1007.

Ben-Porath, I., Thomson, M.W., Carey, V.J., Ge, R., Bell, G.W., Regev, A., and Weinberg, R.A. (2008). An embryonic stem cell-like gene expression signature in poorly differentiated aggressive human tumors. Nat. Genet. *40*, 499–507.

Berman, D.M., Karhadkar, S.S., Hallahan, A.R., Pritchard, J.I., Eberhart, C.G., Watkins, D.N., Chen, J.K., Cooper, M.K., Taipale, J., Olson, J.M., and Beachy, P.A. (2002). Medulloblastoma growth inhibition by hedgehog pathway blockade. Science *297*, 1559–1561.

Blackwood, E.M., and Eisenman, R.N. (1991). Max: a helix-loop-helix zipper protein that forms a sequence-specific DNA-binding complex with Myc. Science *251*, 1211–1217.

Bruggeman, S.W., Valk-Lingbeek, M.E., van der Stoop, P.P., Jacobs, J.J., Kieboom, K., Tanger, E., Hulsman, D., Leung, C., Arsenijevic, Y., Marino, S., and van Lohuizen, M. (2005). Ink4a and Arf differentially affect cell proliferation and neural stem cell self-renewal in Bmi1-deficient mice. Genes Dev. *19*, 1438–1443.

Cho, Y.J., Tsherniak, A., Tamayo, P., Santagata, S., Ligon, A., Greulich, H., Berhoukim, R., Amani, V., Goumnerova, L., Eberhart, C.G., et al. (2011).

Integrative genomic analysis of medulloblastoma identifies a molecular subgroup that drives poor clinical outcome. J. Clin. Oncol. *29*, 1424–1430.

Curley, M.D., Therrien, V.A., Cummings, C.L., Sergent, P.A., Koulouris, C.R., Friel, A.M., Roberts, D.J., Seiden, M.V., Scadden, D.T., Rueda, B.R., and Foster, R. (2009). CD133 expression defines a tumor initiating cell population in primary human ovarian cancer. Stem Cells *27*, 2875–2883.

Eischen, C.M., Weber, J.D., Roussel, M.F., Sherr, C.J., and Cleveland, J.L. (1999). Disruption of the ARF-Mdm2-p53 tumor suppressor pathway in Myc-induced lymphomagenesis. Genes Dev. *13*, 2658–2669.

Ellison, D.W., Onilude, O.E., Lindsey, J.C., Lusher, M.E., Weston, C.L., Taylor, R.E., Pearson, A.D., and Clifford, S.C.; United Kingdom Children's Cancer Study Group Brain Tumour Committee. (2005). beta-Catenin status predicts a favorable outcome in childhood medulloblastoma: the United Kingdom Children's Cancer Study Group Brain Tumour Committee. J. Clin. Oncol. *23*, 7951–7957.

Ellison, D.W., Dalton, J., Kocak, M., Nicholson, S.L., Fraga, C., Neale, G., Kenney, A.M., Brat, D.J., Perry, A., Yong, W.H., et al. (2011a). Medulloblastoma: clinicopathological correlates of SHH, WNT, and non-SHH/WNT molecular subgroups. Acta Neuropathol. *121*, 381–396.

Ellison, D.W., Kocak, M., Dalton, J., Megahed, H., Lusher, M.E., Ryan, S.L., Zhao, W., Nicholson, S.L., Taylor, R.E., Bailey, S., and Clifford, S.C. (2011b). Definition of disease-risk stratification groups in childhood medulloblastoma using combined clinical, pathologic, and molecular variables. J. Clin. Oncol. *29*, 1400–1407.

Frank, A.J., Hernan, R., Hollander, A., Lindsey, J.C., Lusher, M.E., Fuller, C.E., Clifford, S.C., and Gilbertson, R.J. (2004). The TP53-ARF tumor suppressor pathway is frequently disrupted in large/cell anaplastic medulloblastoma. Brain Res. Mol. Brain Res. *121*, 137–140.

Gajjar, A., Chintagumpala, M., Ashley, D., Kellie, S., Kun, L.E., Merchant, T.E., Woo, S., Wheeler, G., Ahern, V., Krasin, M.J., et al. (2006). Risk-adapted craniospinal radiotherapy followed by high-dose chemotherapy and stem-cell rescue in children with newly diagnosed medulloblastoma (St Jude Medulloblastoma-96): long-term results from a prospective, multicentre trial. Lancet Oncol. *7*, 813–820.

Gibson, P., Tong, Y., Robinson, G., Thompson, M.C., Currle, D.S., Eden, C., Kranenburg, T.A., Hogg, T., Poppleton, H., Martin, J., et al. (2010). Subtypes of medulloblastoma have distinct developmental origins. Nature *468*, 1095–1099.

Grandori, C., and Eisenman, R.N. (1997). Myc target genes. Trends Biochem. Sci. *22*, 177–181.

Grandori, C., Cowley, S.M., James, L.P., and Eisenman, R.N. (2000). The Myc/Max/Mad network and the transcriptional control of cell behavior. Annu. Rev. Cell Dev. Biol. *16*, 653–699.

Hemann, M.T., Bric, A., Teruya-Feldstein, J., Herbst, A., Nilsson, J.A., Cordon-Cardo, C., Cleveland, J.L., Tansey, W.P., and Lowe, S.W. (2005). Evasion of the p53 tumour surveillance network by tumour-derived MYC mutants. Nature *436*, 807–811.

Hermeking, H., and Eick, D. (1994). Mediation of c-Myc-induced apoptosis by p53. Science *265*, 2091–2093.

Hoffman, B., and Liebermann, D.A. (2008). Apoptotic signaling by c-MYC. Oncogene *27*, 6462–6472.

Johnson, R.A., Wright, K.D., Poppleton, H., Mohankumar, K.M., Finkelstein, D., Pounds, S.B., Rand, V., Leary, S.E., White, E., Eden, C., et al. (2010). Cross-species genomics matches driver mutations and cell compartments to model ependymoma. Nature *466*, 632–636.

Kamijo, T., Zindy, F., Roussel, M.F., Quelle, D.E., Downing, J.R., Ashmun, R.A., Grosveld, G., and Sherr, C.J. (1997). Tumor suppression at the mouse INK4a locus mediated by the alternative reading frame product p19ARF. Cell *91*, 649–659.

Kenney, A.M., Cole, M.D., and Rowitch, D.H. (2003). Nmyc upregulation by sonic hedgehog signaling promotes proliferation in developing cerebellar granule neuron precursors. Development *130*, 15–28.

Kim, J., Woo, A.J., Chu, J., Snow, J.W., Fujiwara, Y., Kim, C.G., Cantor, A.B., and Orkin, S.H. (2010). A Myc network accounts for similarities between embryonic stem and cancer cell transcription programs. Cell *143*, 313–324.

Knoepfler, P.S., Cheng, P.F., and Eisenman, R.N. (2002). N-myc is essential during neurogenesis for the rapid expansion of progenitor cell populations and the inhibition of neuronal differentiation. Genes Dev. *16*, 2699–2712.

Kool, M., Koster, J., Bunt, J., Hasselt, N.E., Lakeman, A., van Sluis, P., Troost, D., Meeteren, N.S., Caron, H.N., Cloos, J., et al. (2008). Integrated genomics identifies five medulloblastoma subtypes with distinct genetic profiles, pathway signatures and clinicopathological features. PLoS ONE *3*, e3088.

Lam, C.W., Xie, J., To, K.F., Ng, H.K., Lee, K.C., Yuen, N.W., Lim, P.L., Chan, L.Y., Tong, S.F., and McCormick, F. (1999). A frequent activated smoothened mutation in sporadic basal cell carcinomas. Oncogene *18*, 833–836.

Lee, A., Kessler, J.D., Read, T.A., Kaiser, C., Corbeil, D., Huttner, W.B., Johnson, J.E., and Wechsler-Reya, R.J. (2005). Isolation of neural stem cells from the postnatal cerebellum. Nat. Neurosci. *8*, 723–729.

Lee, Y., Miller, H.L., Jensen, P., Hernan, R., Connelly, M., Wetmore, C., Zindy, F., Roussel, M.F., Curran, T., Gilbertson, R.J., and McKinnon, P.J. (2003). A molecular fingerprint for medulloblastoma. Cancer Res. *63*, 5428–5437.

Lumpkin, E.A., Collisson, T., Parab, P., Omer-Abdalla, A., Haeberle, H., Chen, P., Doetzlhofer, A., White, P., Groves, A., Segil, N., and Johnson, J.E. (2003). Math1-driven GFP expression in the developing nervous system of transgenic mice. Gene Expr. Patterns *3*, 389–395.

Malynn, B.A., de Alboran, I.M., O'Hagan, R.C., Bronson, R., Davidson, L., DePinho, R.A., and Alt, F.W. (2000). N-myc can functionally replace c-myc in murine development, cellular growth, and differentiation. Genes Dev. *14*, 1390–1399.

McManamy, C.S., Lamont, J.M., Taylor, R.E., Cole, M., Pearson, A.D., Clifford, S.C., and Ellison, D.W.; United Kingdom Children's Cancer Study Group. (2003). Morphophenotypic variation predicts clinical behavior in childhood non-desmoplastic medulloblastomas. J. Neuropathol. Exp. Neurol. *62*, 627–632.

Northcott, P.A., Korshunov, A., Witt, H., Hielscher, T., Eberhart, C.G., Mack, S., Bouffet, E., Clifford, S.C., Hawkins, C.E., French, P., et al. (2011). Medulloblastoma comprises four distinct molecular variants. J. Clin. Oncol. *29*, 1408–1414.

Pfaff, E., Remke, M., Sturm, D., Benner, A., Witt, H., Milde, T., von Bueren, A.O., Wittmann, A., Schöttler, A., Jorch, N., et al. (2010). TP53 mutation is frequently associated with CTNNB1 mutation or MYCN amplification and is compatible with long-term survival in medulloblastoma. J. Clin. Oncol. *28*, 5188–5196.

Pfister, S., Remke, M., Benner, A., Mendrzyk, F., Toedt, G., Felsberg, J., Wittmann, A., Devens, F., Gerber, N.U., Joos, S., et al. (2009). Outcome prediction in pediatric medulloblastoma based on DNA copy-number aberrations of chromosomes 6q and 17q and the MYC and MYCN loci. J. Clin. Oncol. *27*, 1627–1636.

Raffel, C., Jenkins, R.B., Frederick, L., Hebrink, D., Alderete, B., Fults, D.W., and James, C.D. (1997). Sporadic medulloblastomas contain PTCH mutations. Cancer Res. *57*, 842–845.

Read, T.A., Fogarty, M.P., Markant, S.L., McLendon, R.E., Wei, Z., Ellison, D.W., Febbo, P.G., and Wechsler-Reya, R.J. (2009). Identification of CD15 as a marker for tumor-propagating cells in a mouse model of medulloblastoma. Cancer Cell *15*, 135–147.

Reya, T., Morrison, S.J., Clarke, M.F., and Weissman, I.L. (2001). Stem cells, cancer, and cancer stem cells. Nature *414*, 105–111.

Rich, J.N. (2009). Brain Tumor Stem Cell Markers (New York: Humana Press).

Rios, I., Alvarez-Rodríguez, R., Martí, E., and Pons, S. (2004). Bmp2 antagonizes sonic hedgehog-mediated proliferation of cerebellar granule neurones through Smad5 signalling. Development *131*, 3159–3168.

Romer, J.T., Kimura, H., Magdaleno, S., Sasai, K., Fuller, C., Baines, H., Connelly, M., Stewart, C.F., Gould, S., Rubin, L.L., and Curran, T. (2004). Suppression of the Shh pathway using a small molecule inhibitor eliminates medulloblastoma in Ptc1(+/-)p53(-/-) mice. Cancer Cell *6*, 229–240.

Roussel, M.F., and Hatten, M.E. (2011). Cerebellum development and medulloblastoma. Curr. Top. Dev. Biol. *94*, 235–282.

Schüller, U., Heine, V.M., Mao, J., Kho, A.T., Dillon, A.K., Han, Y.G., Huillard, E., Sun, T., Ligon, A.H., Qian, Y., et al. (2008). Acquisition of granule neuron precursor identity is a critical determinant of progenitor cell competence to form Shh-induced medulloblastoma. Cancer Cell *14*, 123–134.

Silva, J., and Smith, A. (2008). Capturing pluripotency. Cell *132*, 532–536.

Singh, S.K., Hawkins, C., Clarke, I.D., Squire, J.A., Bayani, J., Hide, T., Henkelman, R.M., Cusimano, M.D., and Dirks, P.B. (2004). Identification of human brain tumour initiating cells. Nature *432*, 396–401.

Swartling, F.J., Grimmer, M.R., Hackett, C.S., Northcott, P.A., Fan, Q.W., Goldenberg, D.D., Lau, J., Masic, S., Nguyen, K., Yakovenko, S., et al. (2010). Pleiotropic role for MYCN in medulloblastoma. Genes Dev. *24*, 1059–1072.

Takahashi, K., and Yamanaka, S. (2006). Induction of pluripotent stem cells from mouse embryonic and adult fibroblast cultures by defined factors. Cell *126*, 663–676.

Taylor, M.D., Poppleton, H., Fuller, C., Su, X., Liu, Y., Jensen, P., Magdaleno, S., Dalton, J., Calabrese, C., Board, J., et al. (2005). Radial glia cells are candidate stem cells of ependymoma. Cancer Cell *8*, 323–335.

Thompson, M.C., Fuller, C., Hogg, T.L., Dalton, J., Finkelstein, D., Lau, C.C., Chintagumpala, M., Adesina, A., Ashley, D.M., Kellie, S.J., et al. (2006). Genomics identifies medulloblastoma subgroups that are enriched for specific genetic alterations. J. Clin. Oncol. *24*, 1924–1931.

Todaro, M., Francipane, M.G., Medema, J.P., and Stassi, G. (2010). Colon cancer stem cells: promise of targeted therapy. Gastroenterology *138*, 2151–2162.

Uziel, T., Zindy, F., Xie, S., Lee, Y., Forget, A., Magdaleno, S., Rehg, J.E., Calabrese, C., Solecki, D., Eberhart, C.G., et al. (2005). The tumor suppressors Ink4c and p53 collaborate independently with Patched to suppress medulloblastoma formation. Genes Dev. *19*, 2656–2667.

Wagner, A.J., Kokontis, J.M., and Hay, N. (1994). Myc-mediated apoptosis requires wild-type p53 in a manner independent of cell cycle arrest and the ability of p53 to induce p21waf1/cip1. Genes Dev. *8*, 2817–2830.

Wetmore, C., Eberhart, D.E., and Curran, T. (2001). Loss of p53 but not ARF accelerates medulloblastoma in mice heterozygous for patched. Cancer Res. *61*, 513–516.

Wu, X., Northcott, P.A., Croul, S., and Taylor, M.D. (2011). Mouse models of medulloblastoma. Chin J Cancer *30*, 442–449.

Yang, Z.J., Ellis, T., Markant, S.L., Read, T.A., Kessler, J.D., Bourboulas, M., Schüller, U., Machold, R., Fishell, G., Rowitch, D.H., et al. (2008). Medulloblastoma can be initiated by deletion of Patched in lineage-restricted progenitors or stem cells. Cancer Cell *14*, 135–145.

Zhao, H., Ayrault, O., Zindy, F., Kim, J.H., and Roussel, M.F. (2008). Post-transcriptional down-regulation of Atoh1/Math1 by bone morphogenic proteins suppresses medulloblastoma development. Genes Dev. *22*, 722–727.

Zhu, L., Gibson, P., Currle, D.S., Tong, Y., Richardson, R.J., Bayazitov, I.T., Poppleton, H., Zakharenko, S., Ellison, D.W., and Gilbertson, R.J. (2009). Prominin 1 marks intestinal stem cells that are susceptible to neoplastic transformation. Nature *457*, 603–607.

Zindy, F., Eischen, C.M., Randle, D.H., Kamijo, T., Cleveland, J.L., Sherr, C.J., and Roussel, M.F. (1998). Myc signaling via the ARF tumor suppressor regulates p53-dependent apoptosis and immortalization. Genes Dev. *12*, 2424–2433.

Zindy, F., Knoepfler, P.S., Xie, S., Sherr, C.J., Eisenman, R.N., and Roussel, M.F. (2006). N-Myc and the cyclin-dependent kinase inhibitors p18Ink4c and p27Kip1 coordinately regulate cerebellar development. Proc. Natl. Acad. Sci. USA *103*, 11579–11583.

Zindy, F., Uziel, T., Ayrault, O., Calabrese, C., Valentine, M., Rehg, J.E., Gilbertson, R.J., Sherr, C.J., and Roussel, M.F. (2007). Genetic alterations in mouse medulloblastomas and generation of tumors de novo from primary cerebellar granule neuron precursors. Cancer Res. *67*, 2676–2684.